The phase shift index for marking functional asynchrony in Alzheimer's disease patients using fMRI

Yin Xu[a], Guofan Xu[a], Gaohong Wu[a], Piero Antuono[b], Daniel B. Rowe[a], Shi-Jiang Li[a],*

[a]Department of Biophysics, Medical College of Wisconsin, Milwaukee, WI 53226, USA
[b]Department of Neurology, Medical College of Wisconsin, Milwaukee, WI 53226, USA

Abstract

Our previous study suggested that the functional magnetic resonance imaging MRI (fMRI) COSLOF Index (CI) could be used as a quantitative biomarker for Alzheimer's disease (AD). The fMRI CI was lowest in the AD group (0.13 ± 0.10), followed by the mild cognitive impairment (MCI) group (0.20 ± 0.05) and the control group (0.34 ± 0.09). The current study continues an investigation into which of the following two factors has a dominant role in determining the CI: the signal-to-noise ratio (SNR) or the phase shift of spontaneous low-frequency (SLF) components. By using a theoretical model for SLF components, we demonstrated that the normalized CI does not depend on the SNR of the SLF components. Further analysis shows that by taking the ratio of the cross-correlation coefficient to the maximum-shifted cross-correlation coefficient, the SNR factor can be canceled. Therefore, the determination of the phase shift index (PSI) method is independent of the SNR, and the PSI provides an accurate measure of the phase shift between SLF components. By applying this PSI method to the control, MCI and AD groups of subjects, experimental results demonstrated that the PSI was highest in the AD group ($72.6\pm11.3°$), followed by the MCI group ($58.6\pm5.7°$) and, finally, the control group ($40.6\pm8.4°$). These results suggest that the larger is the PSI value, the more asynchrony exists between SLF components.
© 2008 Elsevier Inc. All rights reserved.

Keywords: fMRI; Alzheimer's disease; functional synchrony; Phase shift index

1. Introduction

Alzheimer's disease (AD), a progressive neurodegenerative disorder characterized by neuritic plaques and neurofibrillary tangles in the human brain, occurs decades before clinical symptoms manifest. Mild cognitive impairment (MCI) is considered the prestage onset of AD, and those with MCI are at greater risk for developing AD [1]. Current research has emphasized the need to determine early biomarkers, thereby facilitating the detection and/or monitoring of early brain changes suggestive of AD and MCI. In addition, it promotes early intervention studies to hinder or slow disease progression [2]. Recent developments in functional magnetic resonance imaging MRI (fMRI) technology with high spatial and temporal resolutions have made it possible to study early AD by noninvasively detecting spontaneous low-frequency (SLF) oscillations (<0.1 Hz) in the hippocampus of the human brain [3]. The hippocampal region is considered to be one of the initial loci for AD. Neuropathological changes are thought to begin in the hippocampal formation and to become severe with disease progression [4,5].

The characteristics of AD progression in the hippocampal region, together with detection of SLF patterns, provide the foundation for the introduction of fMRI indices as a preclinical biomarker for the disease. The previous fMRI index, abbreviated as the COSLOF Index (CI), was introduced to quantify the change in functional synchrony between pairs of voxel time courses. The CI was defined as the mean of the cross-correlation COefficients of Spontaneous LOw Frequency between possible pairs of voxel time courses in the hippocampus of the human brain. We have demonstrated that subjects with AD had a significantly lower CI value than age-matched cognitively healthy elderly subjects.

* Corresponding author. Tel.: +1 414 456 4029; fax: +1 414 456 6512.
E-mail address: sjli@mcw.edu (S.-J. Li).

The current study is a continuation of our previous work that aimed to quantitatively characterize and neurophysiologically understand the CI. There are two factors that may affect the cross-correlation between two voxel time courses: the signal-to-noise ratio (SNR) of SLF components and the phase shift between the two voxel time courses. We will examine how these factors affect the cross-correlation coefficient and the CI. By evaluating the phase shift between the voxel time courses of the SLF components in the hippocampal region, we reveal that the phase shift index (PSI) is a more sensitive marker of AD than the CI.

2. Theory

In a previous study, we utilized the CI in the hippocampal region as a noninvasive biomarker for evaluating the preclinical stage of AD [3]. The CI is calculated from a matrix of the pairwise cross-correlation coefficients of all voxels within a region of interest (ROI). To focus on SLF components, voxel time courses are convolved with a nine-point Hamming filter that has a passband of 0.015–0.1 Hz [3]. According to previous studies [6–8], the SLF component has characteristics of a blood-oxygen-level-dependent (BOLD)-like signal in physiological noise. In a given voxel, the signal at time t is expressed as:

$$s(t) = s_L(t) + n_0(t) \tag{1}$$

where the underlying SLF is $s_L(t)$ and the measurement noise is $n_0(t)$. The cross-correlation coefficient cc_{ij} between the ith and jth voxels ($i,j=1,2,...,K$, $i \neq j$, where K is the number of voxels in the ROI) is calculated between voxel time courses $s_i(t)$ and $s_j(t)$ as:

$$cc_{ij} = \frac{\sum_{t=1}^{N}(s_i(t)s_j(t))}{\sqrt{\sum_{t=1}^{N}(s_i(t))^2}\sqrt{\sum_{t=1}^{N}(s_j(t))^2}}$$

$$= \frac{\sum_{t=1}^{N}(s_i(t)s_j(t))}{\hat{\sigma}_i \hat{\sigma}_j} \tag{2}$$

with $t=1,...,N$. In Eq. (2), it is generically assumed that the voxel time courses have a mean of zero and are demeaned following filtering. The previously published CI that has been established as a preclinical biomarker for AD is defined as:

$$CI = \frac{2}{K(K-1)} \sum_{i,j=1,i>j}^{K} cc_{ij}. \tag{3}$$

Two factors may affect the cross-correlation between two voxel time courses: the SNR of SLF components and the phase shift between the two voxel time courses. First, we examine the variation in the ratio of the SLF components to thermal noise and determine how a change in them might produce modifications in the cross-correlations and, hence,

CIs. In the model presented in Eq. (1), the mean and variance of $s_L(t)$ are assumed to be zero and σ_L^2; and the mean and variance of $n_0(t)$ are assumed to be zero and σ_0^2. The two components s_L and n_0 are independent, so that $cov(s_L,n_0)=0$. The cross-correlation in Eq. (2) turns out to be:

$$cc_{ij} = \frac{\hat{\sigma}_{ij}}{\sqrt{(\hat{\sigma}_{Li}^2 + \hat{\sigma}_{0i}^2)(\hat{\sigma}_{Lj}^2 + \hat{\sigma}_{0j}^2)}} \tag{4}$$

where $\hat{\sigma}_{ij}$ is the sample covariance between voxels i and j, while $\hat{\sigma}_i^2 = \hat{\sigma}_{Li}^2 + \hat{\sigma}_{0i}^2$ and $\hat{\sigma}_j^2 = \hat{\sigma}_{Lj}^2 + \hat{\sigma}_{0j}^2$ are the sample variances in voxels i and j with constituents $\hat{\sigma}_L^2$ and $\hat{\sigma}_0^2$ due to the SLF components and thermal noise. It is immediately apparent that the thermal noise variance $\hat{\sigma}_0^2$ that is estimated in each voxel and is stochastically equivalent will affect the cross-correlation coefficient. According to Eq. (4), a higher SNR, $\eta = \hat{\sigma}_L/\hat{\sigma}_0$, may lead to higher cross-correlation coefficients and higher CIs. Since the SNR is a subject/scan-specific factor, it may affect a comparison of the CIs between subjects or between groups of subjects.

Based on this characteristic of SLF components in the SNR, a cross-correlation coefficient without the impact of SNR variation can be obtained by normalizing the cc_{ij} to noise $\hat{\sigma}_0^2$ in Eq. (4). The normalized cross-correlation coefficient ncc_{ij} is defined as:

$$ncc_{ij} = cc_{ij} \frac{\sqrt{\hat{\eta}_i^2 + 1} \cdot \sqrt{\hat{\eta}_j^2 + 1}}{\hat{\eta}_i \cdot \hat{\eta}_j} \tag{5}$$

and the normalized CI (nCI) can be estimated as:

$$nCI = \frac{2}{K(K-1)} \sum_{i,j=1,i>j}^{K} \left(cc_{ij} \frac{\sqrt{\hat{\eta}_i^2 + 1} \cdot \sqrt{\hat{\eta}_j^2 + 1}}{\hat{\eta}_i \cdot \hat{\eta}_j} \right). \tag{6}$$

To reduce the complexity of the computation, we assume that the SNR η_m is identical in all voxel time courses within an ROI and is obtained as a sample mean SNR over the ROI as:

$$\hat{\eta}_m = \frac{1}{K} \sum_{i=1}^{K} \hat{\eta}_i. \tag{7}$$

Then, the nCI in Eq. (6) is approximately simplified as:

$$nCI \approx \frac{\hat{\eta}_m^2 + 1}{\hat{\eta}_m^2} \cdot \frac{2}{K(K-1)} \cdot \sum_{i,j=1,i>j}^{K} cc_{ij}. \tag{8}$$

The validation of these approximations is provided by Monte Carlo simulations in Appendix B.

Another factor that may affect the cross-correlation between two voxel time courses is the phase shift. To estimate the phase shift, we first model the SLF components by assuming that two voxel time courses contain an identical

frequency component f_c. The ith voxel time course in Eq. (1) becomes:

$$s_i(t) = \eta_i \sqrt{2} \sigma_0 \sin(2\pi f_c \cdot t + \theta_i) + n_i(t) \qquad (9)$$

where η_i is the SNR, θ_i is the phase of the frequency f_c and σ_0 is the standard deviation of thermal noise. Then, the phase shift between the SLF signals in two voxel time courses can affect the value of the cross-correlation. With this simplification, Eq. (4) can be rewritten as:

$$cc_{ij} = \frac{\eta_i \eta_j \cdot \cos(\theta_{ij})}{\sqrt{\eta_i^2 + 1} \cdot \sqrt{\eta_j^2 + 1}} \qquad (10)$$

where θ_{ij} is the phase shift between SLF signals and is equal to $|\theta_i - \theta_j|$. Full synchrony between two signals (i.e., the zero phase shift between SLF components) can be reached by shifting one voxel time course by τ^m. Here, τ^m is the number of time points shifted to obtain a maximum cross-correlation between voxel time courses i and j, as shown below:

$$\tau^m = \arg\left(\max_{0 < \tau < T} \frac{\sum_{t=1}^{N} (s_i(t) \cdot s_j(t + \tau))}{\sqrt{\eta_i^2 + 1} \cdot \sqrt{\eta_j^2 + 1}} \right), \qquad 0 < \tau < \frac{1}{f_L} \qquad (11)$$

where f_L=0.015 Hz, which is the lower limit of the passband of the filter, and T is $1/f_L/T_R$ (where T_R is the repetition time of acquisition). Then, the maximum-shifted cross-correlation coefficient (cc^m) becomes:

$$cc_{ij}^m = \frac{\sum_{t=1}^{N} (s_i(t) s_j \cdot (t + \tau^m))}{\sqrt{\eta_i^2 + 1} \cdot \sqrt{\eta_j^2 + 1}}$$
$$= \frac{\eta_i \eta_j}{\sqrt{\eta_i^2 + 1} \cdot \sqrt{\eta_j^2 + 1}} \qquad (12)$$

where we still assume that the SLF signal is a single sinusoid function. Combining Eqs. (10) and (12), the phase shift can be recovered immediately as:

$$\hat{\theta}_{ij} = \cos^{-1}\left(\frac{cc_{ij}}{cc_{ij}^m} \right). \qquad (13)$$

For ROI evaluation, the phase shift can be estimated as:

$$\hat{\theta}_G = \overline{\theta_{ij}} = \frac{2}{K(K-1)} \sum_{i,j=1,i\neq j}^{K} \cos^{-1}\left(\frac{cc_{ij}}{cc_{ij}^m} \right). \qquad (14)$$

To minimize the effect of nonuniformity of SNR on real data, it is suggested that the ROI phase shift be calculated as follows:

$$\hat{\theta}_G \approx \cos^{-1}\left(\frac{CI}{CI^m} \right), CI^m = \frac{2}{K(K-1)} \sum_{i,j=1,i>j}^{K} cc_{ij}^m \qquad (15)$$

where CI^m is defined as the maximum-shifted COSLOF. The validation of this approximation between Eqs. (14) and (15) is provided by the theoretical derivation and Monte Carlo simulations in Appendix B.

The ROI estimate in Eq. (14) is named the PSI to quantify the regional phase shift. Clearly, a larger phase shift leads to lower cross-correlation coefficients; for an ROI, a larger PSI leads to a lower CI value. It is also noteworthy that the PSI is a normalized index and is not sensitive to noise factors because the ratio of CI to CI^m canceled the noise factor in Eqs. (10) and (12).

The above derivations are made based on the assumption that the SLF components in two voxel time courses contain an identical frequency component with different phases. In reality, the SLF signal could contain more than one frequency component. Then, the ith voxel time course in Eq. (1) can be decomposed as:

$$s_i(t) = \sum_{f \in F} \eta_f \sqrt{2} \sigma_0 \sin(2\pi f \cdot t + \theta_i(f)) + n_i(t) \qquad (16)$$

where f is the frequency bin, F is the set of available frequencies for SLF signal, η_f is the uniform SNR of the SLF component for frequency f, $\theta_i(f)$ is the phase of f and σ_0 is the standard deviation of thermal noise. Thus, Eq. (10) becomes:

$$cc_{ij} = \frac{\sum_{f \in F} \eta_f^2 \cos(\theta_{ij}(f))}{\sum_{f \in F} \eta_f^2 + 1} \qquad (17)$$

where $\theta_{ij}(f)$ is the phase shift for frequency f [i.e., $|\theta_i(f) - \theta_j(f)|$] between two voxel time courses.

If $|\theta_i(f) - \theta_j(f)|$ is zero for all frequency components by shifting one voxel time course at τ^m, the maximum-shifted cross-correlation coefficient in Eq. (12) turns out to be:

$$cc_{ij}^m = \frac{\sum_{f \in F} \eta_f^2}{\sum_{f \in F} \eta_f^2 + 1}. \qquad (18)$$

Combining Eqs. (17) and (18), the phase shift estimated in Eq. (13) becomes:

$$\hat{\theta}_{ij} = \cos^{-1}\left(\frac{cc_{ij}}{cc_{ij}^m} \right) = \cos^{-1}\left(\frac{\sum_{f \in F} \eta_f^2 \cos(\theta_{ij}(f))}{\sum_{f \in F} \eta_f^2} \right). \qquad (19)$$

In practice, due to the limited length of the voxel time courses, cc_{ij}^m is obtained by experimentally shifting one voxel time course at τ^m, and the obtained $\hat{\theta}_{ij}$ is considered an equivalent phase shift.

For ROI evaluation, the estimation of the phase shift in the presence of many frequency components in SLF

components can be estimated according to Eqs. (14) and (15). In this study, the parameters of the CI, nCI and PSI are all estimated and employed to distinguish the differences among the AD, MCI and control groups.

3. Materials and methods

3.1. Human subjects

Fourteen AD patients (age, 72±6 years), eight subjects with MCI (age, 69±3 years) and 13 cognitively healthy controls (age, 68±4 years) were recruited from the Memory Disorders Clinic at the Medical College of Wisconsin (Milwaukee, WI). Informed consent was obtained from all subjects for this institutional-review-board-approved study. The detailed inclusion and exclusion criteria for the three groups of subjects (AD, MCI and control) and the diagnoses of probable/possible AD and MCI subjects have been described previously [3]. All cognitively healthy subjects underwent a set of cognitive examinations; none reported subjective symptoms of cognitive impairment (their Mini Mental Status Examination scores were ≥27/30, and their modified Hachinski scores were ≤4). fMRI was performed within a maximum of 2 months of cognitive testing.

3.2. fMRI

fMRI data acquisition was conducted on a GE Signa 1.5-T scanner (GE Medical Systems, Milwaukee, WI) using a local gradient coil and an end-capped birdcage radio-frequency coil. Foam padding was used to limit head motion within the head coil. A single-shot gradient-echo Echo Planar Imaging (EPI) sequence in the sagittal plane was used with the following imaging parameters: T_R=2 s, T_E=40 ms, field of view=24 cm, slice thickness=7 mm, matrix=64×64. Fifteen sagittal slices and 180 images per slice were obtained in 6 min. In all MRI sessions, the corresponding 256×256 T_1-weighted 3D Spoiled Gradient Recalled Echo (SPGR) anatomic images were also acquired. During scanning, all subjects were in resting state (performing no task, with eyes closed).

3.3. Data analysis

All functional datasets were preprocessed to detect motion and to remove linear trends. Four AD patients and four controls were excluded from further data processing due to excessive motion (>1 mm). The detailed procedures used to locate the hippocampal region and to select the hippocampal voxels from the EPI dataset have been previously described in detail [3,9]. Specifically, the left and right hippocampi were manually identified on T_1-weighted 3D SPGR images according to Duvernoy [10]. The most anterior boundary of the hippocampus adjoins the ventral border of the amygdala, and the dorsal border is formed by the dorsal cerebrospinal fluid (CSF) of the temporal (inferior) horn of the lateral ventricle and alveus. Its ventral border is formed by the white matter of the parahippocampal gyrus. The posterior CSF and choroid plexus of the trigone of the lateral ventricle form the dorsal and posterior border of the hippocampus. Tracing was performed on all relevant sagittal slices with a mouse-controlled cursor, with boundaries displayed in real time on
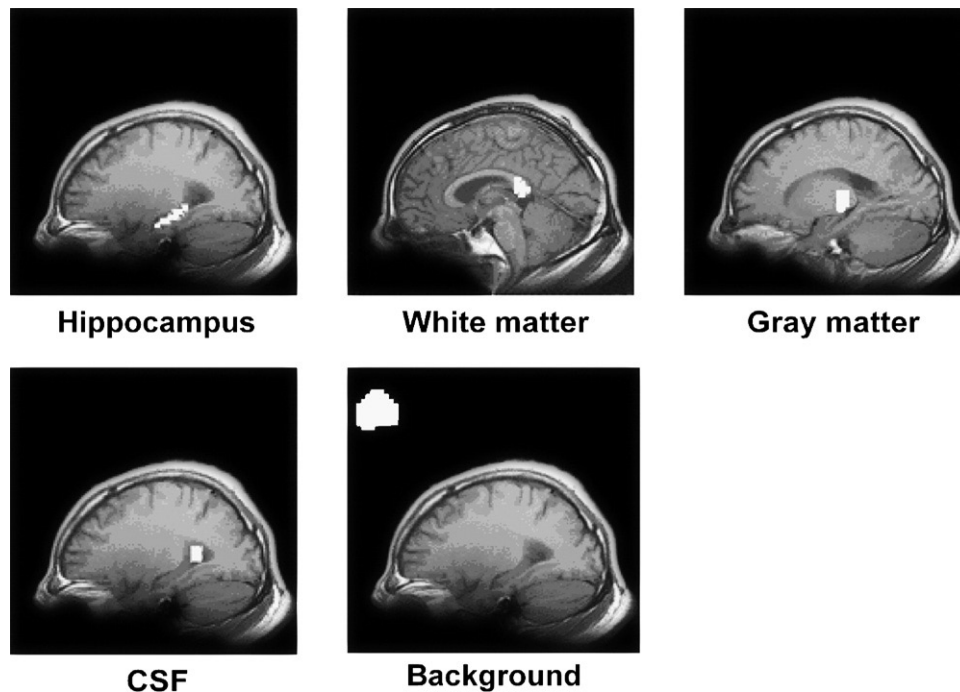

Fig. 1. The representative regions (in white) selected for analysis: the hippocampus, white matter, gray matter, CSF and the outside brain region of a subject. The selected regions are mapped onto T_1-weighted anatomical images.

the MRI slices. In addition, they were displayed in the remaining orthogonal slices. Then, these masks were transformed to the Talairach space. Since the spoiled Gradient Recalled Echo (GRE) images had 1.1-mm spatial resolution and the functional MR images had 3.75-mm spatial resolution, the voxels included in the hippocampal region in the functional MR images were determined according to the masked volume in the 3D SPGR images using a deresolution program. (Note that functional MR images were also transformed into the Talairach space.) Only those voxels in functional MR images that contained >50% of the masked 3D SPGR voxels were included for the voxel time course analysis.

To extract the SLF components, the original time courses were filtered with a nine-point Hamming band-pass filter with a passband of 0.015–0.1 Hz. To compare the SNRs in different brain regions, five regions in fMRI datasets were selected: the left and right hippocampi, white matter from the splenium of the corpus callosum, gray matter from the thalamus, CSF (lateral ventricle) and a pure-noise region outside the brain region, as shown in Fig. 1. Within the same slice containing the hippocampal region, three voxels in different (CSF) regions were selected as regression vectors in order to remove CSF motion and potential aliased cardiac pulsations [11]. The voxel time courses in the left and right hippocampal regions were employed to calculate the CI, nCI and PSI for each of the control, MCI and AD groups.

After exclusion due to motion, the remaining subjects in the study were 9 control subjects (3 men, 70±3 years; 6 women, 70±7 years), 10 AD patients (5 men, 73±5 years; 5 women, 71±10 years) and 8 MCI subjects (6 men, 74±3 years; 2 women, 66±2 years).

3.4. Determination of thermal noise

It is known that the thermal noise in magnitude MR images is Rician distributed. Furthermore, the Rician distribution is reduced to Rayleigh distribution when the signal is zero (e.g., outside the brain region on MR images). When the signal level is very large (e.g., inside the brain region on MR images), the Rician distribution can be approximated as Gaussian distributed. However, for fMRI scans, variations in voxel time courses in the brain regions contain not only thermal noise but also other temporal variations such as physiologic noise. This makes it very difficult to estimate the standard deviation of thermal noise $\hat{\sigma}_0$. Therefore, in the present study, we estimate the thermal noise standard deviation $\hat{\sigma}_0$ in two steps. In the first step, voxel time courses outside the brain region at the upper left corner of the image are manually selected to estimate the Rayleigh-distributed noise standard deviation $\hat{\sigma}_R$. The standard deviation of noise $\hat{\sigma}_R$ is then converted to the Gaussian-distributed thermal noise standard deviation $\hat{\sigma}_{M-noise}$ with a correction factor according to Gudbjartsson and Patz [12]. In the second step, the estimated Gaussian

noise standard deviation $\hat{\sigma}_M$ is then scaled by the norm of the Hamming filter to adjust for smoothing:

$$\hat{\sigma}_0 = \hat{\sigma}_{M-noise} \cdot \left(\sum_t h^2(t) \right)^{1/2} \tag{20}$$

where $h(t)$ represents the time-domain nine-point Hamming filter coefficients. Then, the standard deviation of the SLF in the hippocampal region can be calculated as:

$$\hat{\sigma}_L = \sqrt{\hat{\sigma}_{M-hipp}^2 - \hat{\sigma}_0^2} \tag{21}$$

where $\hat{\sigma}_{M-hipp}$ is the mean of the estimated temporal standard deviation of the voxel time courses in the hippocampus. Based on Eqs. (20) and (21), the SNR can be estimated as $\hat{\eta} = \hat{\sigma}_L/\hat{\sigma}_0$.

3.5. Coherence and phase delay

In addition to the CI and proposed PSI, coherence and phase delay were implemented and applied to our datasets to evaluate temporal correlation between voxel time courses. The coherence ρ between two voxel time courses [13–15] was estimated as follows:

$$\hat{\rho}_{ij} = \sum_{f=f_L}^{f_H} \hat{\rho}_{ij}(f) = \sum_{f=f_L}^{f_H} \frac{|S_{ij}(f)|}{\sqrt{S_{ii}(f)S_{jj}(f)}} \tag{22}$$

where $S_{ii}(f)$ and $S_{jj}(f)$ are the spectral power on the frequency component f of the ith and jth voxel time courses, respectively; $S_{ij}(f)$ is the cross-spectral power; f_L is the lower frequency bound of SLF set to 0.015 Hz; and f_H is the upper frequency bound set to 0.1 Hz. ROI coherence is simply the average of the coherences between each pair of voxel time courses. The phase delay τ can be estimated as [15]:

$$\hat{\tau}_{ij} = \left| \frac{\sum_{f=f_L}^{f_H} \varphi_{ij}(f)}{2\pi \sum_{f=f_L}^{f_H} f} \right|, \quad \varphi_{ij}(f) = \tan^{-1} \left(\frac{\text{Im}(S_{ij}(f))}{\text{Re}(S_{ij}(f))} \right). \tag{23}$$

At par with ROI coherence, ROI phase delay is simply the average of the phase delays between each pair of voxel time courses.

Table 1
The SNRs in four selected regions of three subject groups

(A) SNR (mean±S.D.)			
Region	AD	MCI	Control
Hippocampus	2.75±0.61	2.60±1.23	2.00±0.45
White matter	1.24±0.40	1.00±0.28	0.71±0.18
Gray matter	1.45±0.70	1.57±0.79	1.04±0.25
CSF	4.29±0.85	3.16±0.33	3.78±0.45

(B) One-way unbalanced ANOVA for the SNR in the hippocampal region of three subject groups		
	$F_{(2,23)}$	P
SNR in hippocampus	1.861	.1783

4. Results

The SNRs in the hippocampal region for the three groups of subjects are presented in Table 1. The SNRs in the

Table 2
Statistical comparison between oCIs and nCIs in five brain regions of three subject groups

(A) oCIs (mean±S.D.)

Region	AD	MCI	Control
Hippocampus^{nr}	0.127±0.095	0.196±0.051	0.341±0.085
Hippocampus^{rg}	0.142±0.090	0.171±0.055	0.304±0.065
White matter	0.088±0.059	0.138±0.092	0.108±0.123
Gray matter	0.175±0.062	0.134±0.077	0.176±0.112
CSF	0.069±0.052	0.094±0.071	0.079±0.033
Pure-noise region	0.004±0.006	0.003±0.003	0.005±0.006

(B) nCIs (mean±S.D.)

Region	AD	MCI	Control
Hippocampus^{nr}	0.147±0.106	0.277±0.052	0.437±0.079
Hippocampus^{rg}	0.164±0.099	0.236±0.065	0.395±0.084
White matter	0.172±0.080	0.271±0.154	0.287±0.212
Gray matter	0.382±0.233	0.233±0.117	0.346±0.175
CSF	0.072±0.054	0.103±0.078	0.085±0.036

(C) One-way unbalanced ANOVA for CIs and nCIs in the hippocampus of three subject groups

Parameter	$F_{nr}(2,23)$	P_{nr}	$F_{rg}(2,23)$	P_{rg}
CI	14.563	<.0001	11.055	.0004
nCI	24.316	<.0001	15.453	<.0001

(D) Pairwise (one-tailed) t test between three subject groups

Group	P
CI^{nr}	
AD vs. MCI	.0513
MCI vs. CONTROL **	.0006
AD vs. CONTROL ***	.0001
CI^{rg}	
AD vs. MCI	.2365
MCI vs. CONTROL **	.0003
AD vs. CONTROL ***	.0005
nCI^{nr}	
AD vs. MCI *	.0494
MCI vs. CONTROL ***	.0001
AD vs. CONTROL ***	<.0001
nCI^{rg}	
AD vs. MCI	.0566
MCI vs. CONTROL **	.0004
AD vs. CONTROL ***	<.0001

(E) Kruskal–Wallis nonparametric tests for the CIs and nCIs of three subject groups

Parameter	H_{nr}	P_{nr}	H_{rg}	P_{rg}
CI	14.508	.0007	11.164	.0038
nCI	17.616	.0001	14.829	.0006

nr — no CSF voxel regression; rg — with CSF voxel regression.
The CIs presented in all other regions in this article have been calculated without CSF voxel regression.
 * $P<.05$.
 ** $P<.01$.
 *** $P<.001$.

hippocampal regions for the AD, MCI and control groups are 2.75±0.61, 2.60±1.23 and 2.00±0.45, respectively. One-way unbalanced analysis of variance (ANOVA) data show no significant differences in SNRs in the hippocampal regions among the groups [$F(2,23)=1.861$, $P=.1783$]. The obtained hippocampus volumes (the sum of both sides) for the three subject groups are as follows: 5.68±1.24 cm^3 for the control group, 5.60±0.31 cm^3 for the MCI group and 4.62±1.17 cm^3 for the AD group. The one-way unbalanced ANOVA data show no significant differences in volumes among the groups [$F(2,23)=2.855$, $P=.1122$].

Table 2 lists the original CIs (oCIs) and nCIs and their statistical differences in the five regions for the control, MCI and AD groups, based on Eqs. (3) and (6). Table 2A shows the oCIs, and Table 2B shows the nCIs in the five brain regions of the AD, MCI and control groups. One-way unbalanced ANOVA indicates that both the oCIs [$F(2,23)=14.563$, $P<.0001$] and the nCIs [$F(2,23)=24.316$, $P<.00001$] are significantly different in the three groups. The CI is largest for the control group, moderate for the MCI group and lowest for AD patients. Except in the case of AD versus MCI, CSF voxel regression does not significantly alter the statistical results, either in ANOVA or in one-tailed t tests. Table 2D shows that the pairwise t test results for both oCIs and nCIs have significant statistical power to separate the AD-versus-control groups and the MCI-versus-control groups. However, the ability of the CI to distinguish between the MCI and AD groups was moderate and became insignificant when CSF regression was employed. Further Z-statistical analysis revealed that the Z-score necessary for the oCI to separate the MCI group from the control group was 3.215, and the score necessary to separate the AD group from the control group was 3.676. The Z-score necessary for the nCI to separate the MCI group from the control group was 3.571. The Z-score used to separate the AD group from the control group was 4.286. The discriminating power of the nCI was stronger than that of the oCI.

Since the distribution of the oCIs or nCIs is not assured to be Gaussian, nonparametric Kruskal–Wallis tests were conducted as a general statistical evaluation. As listed in Table 2E, the oCIs and nCIs can significantly detect the differences among the three groups (oCIs, $H=14.508$, $P=.0007$; nCIs, $H=17.616$, $P=.0001$).

Based on Eqs. (10), (12) and (15), Table 3 lists the maximum-shifted CI (CI^m) and the PSI (θ_G), as well as the results of statistical comparisons for the PSI in the hippocampal region between the control, MCI and AD groups. Table 3A illustrates that the CI^m values are comparably similar in each of the five regions between the three groups, while the PSI values in the hippocampal region in the three subject groups are significantly different, as listed in Table 3B. The PSI without CSF voxel regression is largest (72.6±11.3°) for the AD group. It is smallest (40.6±8.4°) for the control group, and the value is 58.6±5.7° for the MCI group. The larger is the PSI, the less synchrony there is between the voxel time courses in the hippocampal region. In

Table 3
Statistical comparisons between maximum-shifted CIs and PSI in five brain regions of three subject groups

(A) CI^m (mean±S.D.)

Region	AD	MCI	Control
Hippocampus^{nr}	0.412±0.075	0.390±0.072	0.438±0.054
Hippocampus^{rg}	0.398±0.061	0.362±0.054	0.424±0.037
White matter	0.304±0.049	0.305±0.056	0.280±0.067
Gray matter	0.336±0.063	0.331±0.083	0.325±0.055
CSF	0.307±0.051	0.337±0.069	0.282±0.025
Pure-noise region	0.233±0.003	0.234±0.006	0.232±0.002

(B) θ_G (mean±S.D.)

Region	AD	MCI	Control
Hippocampus^{nr}	72.6±11.3	58.6±5.7	40.6±8.4
Hippocampus^{rg}	68.0±14.1	58.9±7.0	43.5±10.1
White matter	74.1±9.2	64.4±14.7	77.9±4.5
Gray Matter	60.5±9.8	67.1±11.5	70.7±9.7
CSF	78.1±7.9	73.8±6.2	74.0±12.3
Pure-noise region	88.9±1.6	88.2±0.9	88.5±1.5

(C) One-way unbalanced ANOVA for the CI^m and $\grave{e}_G$ of three subject groups

Parameter	$F_{nr}(2,23)$	P_{nr}	$F_{rg}(2,23)$	P_{rg}
CI^m	0.941	.4049	2.661	.0913
θ_G	25.789	<.0001	10.462	.0006

(D) Pairwise (one-tailed) t test between three subject groups

Group	P
PSI^{nr}	
AD vs. MCI **	.0047
MCI vs. CONTROL **	.0001
AD vs. CONTROL ***	<.0001
PSI^{rg}	
AD vs. MCI	.1487
MCI vs. CONTROL **	.0006
AD vs. CONTROL ***	.0006

(E) Kruskal–Wallis nonparametric tests for the CI^m and $\grave{e}_G$ of three subject groups

Parameter	H_{nr}	P_{nr}	H_{rg}	P_{rg}
CI^m	2.459	.2924	4.073	.1305
θ_G	17.939	.0001	11.478	.0032

nr — no CSF voxel regression; rg — with CSF voxel regression.
The CIs presented in all other regions in this article have been calculated without CSF voxel regression.
    *P<.05.
    ** P<.01.
    *** P<.001.

Table 3C, one-way unbalanced ANOVA shows a statistically significant difference in PSI values among the three groups of hippocampal regions [$F(2,23)$=25.789, P<0001]. Table 3D shows the pairwise t test results among the three groups. Although CSF regression has reduced P values, the differences between the control-versus-MCI groups and the control-versus-AD groups are still significant. Z-statistical differences are significant between the MCI and control groups (Z=3.672) and between the AD and control groups (Z=4.365).

Again, since the distribution of the maximum-shifted CI (CI^m) and the PSI (θ_G) cannot be assured to be Gaussian, nonparametric Kruskal–Wallis tests were conducted. Significant differences in PSI values among the three groups were detected (H=17.939, P=.0001), while maximum-shifted CIs (CI^m) were not significantly different among the three subject groups (H=2.459, P=.2924).

5. Discussion

The present study consists of two parts: the first part provides a model of SLF components to investigate how SNR distributions could affect the calculations of cross-correlation coefficients and the CI, and the second part applies this model to analyze the functional synchrony in the hippocampal region of the normal, MCI and AD subjects. In regard to the first part, our simulation study showed that SNR variations significantly affect the CI calculation. The lower is the SNR, the higher is the error for the CI. By normalizing the SNR factor, this error can be significantly reduced, and the nCI is no longer affected by the SNR factor. Therefore, the nCI has a stronger discriminating power than the oCI. However, accurate SNR estimation is susceptible to background artifacts and temporal changes in the brain region. As a result, the method of normalizing the SNR factor is not ideal for providing an optimal measurement of the CI. To overcome this problem, we further developed the PSI method.

Ideally, if there is no thermal noise present, the cross-correlation coefficient between two signals reflects the phase shift (the angle between two vectors). However, when thermal noise is present, the variable SNR can affect the cross-correlation coefficient and make it less reliable in detecting the phase shift, in turn affecting the CI calculation. Our simulation study demonstrated that the inaccuracy of the SNR estimation can be avoided through the cancellation of the SNR factor, by taking the ratio of the cross-correlation coefficient to the maximum-shifted cross-correlation coefficient, as shown in Eqs. (10), (12) and (13). Therefore, no matter what the SNR is, the PSI method provides an accurate measure of the phase shift between the SLF components. As a result, the PSI measurement provides a stronger discriminatory power than the original and normalized COSLOF methods.

For the second part of study, we applied the model of the oCI, nCI and PSI methods to investigate the functional synchrony in the hippocampus of the normal, MCI and AD subjects. We have demonstrated that the nCI and the PSI, quantified by θ_G, have higher statistical discriminatory power between these groups of subjects than the oCI based on their Z-score comparisons. A large PSI value in the hippocampal region of the AD and MCI subjects reveals a significantly large phase shift among voxel time courses, indicating asynchrony.

Unlike thermal noise, which is not correlated and can be canceled when calculated with the PSI, an aliased cardiac
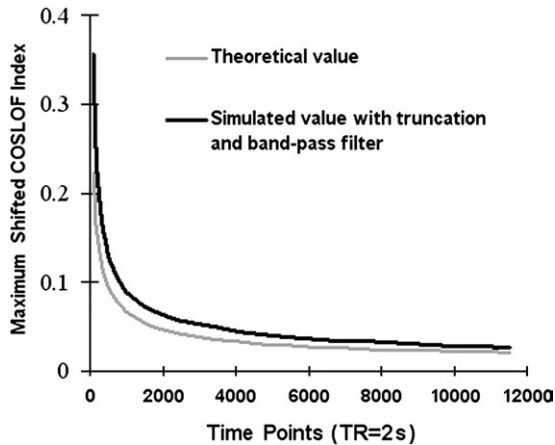
Fig. 2. The relationship between the number of time points and the maximum-shifted cross-correlation coefficient $cc^m(0)$ between two noise time courses with standard normal distribution. The lighter gray line represents the theoretical value, and the dark line represents the simulated value.

signal cannot be canceled because it can be cross-correlated as "signal." With a T_R of 2 s, the cardiac component can be aliased into the frequency range of the SLF signal (0.015–0.1 Hz) and may affect the calculation of the PSI. Since we did not simultaneously record the cardiac pulse during fMRI scanning and could not employ a retrospective correction technology [16,17], we employed the CSF signal as a regressor to test whether the cardiac signal played a significant role. The CSF signal usually contains the aliased cardiac signal due to the steady-state free precession mechanism [18]. As demonstrated in Table 3C, the significance values in the PSI measurement estimated with ANOVA were not altered with or without CSF regression. In addition, the significance values in the PSI between the MCI-versus-control groups and the AD-versus-control groups were not altered with or without CSF regression (Table 3D). Therefore, this potential confounding factor did not play an important role in estimating the PSI. However, CSF regression did affect the significance between the MCI and AD groups. The reason is not known. One possibility is that the CSF voxel time courses may contain other unknown signal sources, which might introduce uncertainty to PSI estimations. We do not recommend the

CSF regression method. Rather, the retrospective correction technology should be employed [16,17].

Respiratory signals may also be present in fMRI voxel time courses. Its frequency usually lies within the range 0.1–0.3 Hz [19,20]. With a T_R of 2 s, this respiratory frequency could fold over into the frequency range of 0.1–0.25 Hz, which is outside the Hamming filter passband. Therefore, the respiratory frequency generally does not contribute as a confounding factor.

Respiratory variation in volume (i.e., variation in arterial CO_2 level, which acts as a vasodilator) could also induce BOLD signal variation. The spectral density of this temporal variation in BOLD signal appears at about 0–0.05 Hz [18,19], which resides in the frequency range of SLF signals, hence imposing a potential confounding factor for PSI calculations. The respiratory variations in volume were region specific, and the most affected regions were the posterior cingulate and precuneus, while the hippocampal region seemed immune to this variation [19]. Furthermore, a recent study on the functional synchrony analysis of the parahippocampal region also showed that different cognitive tasks lead to different PSI values [21], implying that it is unlikely for respiratory variation to play significant roles in both cases. Nevertheless, it will be necessary to record and regress this respiratory variation in future studies.

It is interesting to note that the maximum-shifted CI (CI^m) in the pure-noise region shown in Table 3A is about 0.23 and is similar in the three study groups. Intuitively, the cross-correlation coefficient between noise time courses should be close to zero. The noticeably shifted cross-correlation coefficient of 0.23 for noise is explained below. As described in detail in Appendix A and as shown in Fig. 2, the relationship between the number of time points M and $cc^m(\eta)$ theoretical calculation and simulation showed that the value of $cc^m(\eta)$ depends on the number of time points M in a voxel time course. The larger M is, the smaller $cc^m(\eta)$ is. As shown in Table 4, after truncation and band-pass filtering, the simulated $cc^m(\eta)$ for noise is about 0.23 when M is 180. The simulated data are consistent with experimental results.

As we have demonstrated, the PSI, with its cancelled noise factor, has a much stronger statistical power than the CI. Nevertheless, a certain level of SNR is necessary to

Table 4

The relationships between the number of time points and the maximum-shifted cross-correlation of white normal noise $cc^m(0)$ under different conditions

Time points (scanning time)	Theoretical $cc^m(0)$	Simulated $cc^m(0)$	Simulated $cc^m(0)$ with truncation	Simulated $cc^m(0)$ with band-pass filter	Simulated $cc^m(0)$ with truncation and band-pass filter
90 (3 min)	0.2221	0.2150	0.2740	0.2981	0.3554
180 (6 min)	0.157	0.1562	0.1663	0.2110	0.2307
360 (12 min)	0.111	0.1114	0.1207	0.1453	0.1563
720 (24 min)	0.0785	0.0792	0.0786	0.1044	0.1077
1440 (48 min)	0.0555	0.0553	0.0564	0.0730	0.0745
2880 (96 min)	0.0392	0.0389	0.0391	0.0522	0.0529
5760 (192 min)	0.0277	0.0279	0.0280	0.0367	0.0363
11,520 (384 min)	0.0204	0.0192	0.0198	0.0252	0.0256

reliably calculate the PSI. As shown in Appendix A, the minimum SNR for a reliable calculation of the PSI was estimated to be approximately 1. It is conceivable that the SNR for a 3-T scanner will certainly be higher than that for a 1.5-T scanner, resulting in a more reliable estimation of PSI.

In addition, there are other methods that can be used to study the association between time series, such as coherence analysis (frequency-domain correlation) [13,14]. The phase delay, according to its conventional meaning, has also been developed without the use of a band-pass filter [15]. However, these methods are vulnerable to the lower SNR and complex spectrum. The SNR for SLF components is relatively low, as listed in Table 1. We have applied both coherence and phase delay methods to our experimental data. The estimated coherences for the control, MCI and AD groups are 0.43±0.08, 0.37±0.05 and 0.34±0.11, respectively; the phase delay for the control, MCI and AD groups are 0.95±0.10, 0.94±0.08 and 1.03±0.13 s, respectively. There is no significant difference between each pair. This is also true for ANOVA statistics. Therefore, we prefer the PSI to the coherence or phase delay method in this study. We have examined how the SNR of SLF components and the phase shift between the two voxel time courses affect the cross-correlation coefficient and the CI. It is reasonable to ask how the spectral density of the SLF components would affect the correlation analysis. However, the spectral densities of the SLF components are rather complex because not all frequency components in SLF components contribute to the calculation of the cross-correlation coefficients between voxel time courses. In addition, those frequency components contribute to the different cross-correlation coefficients from different pairs of voxel time courses. Therefore, the concept of spectral density influencing the calculation of the cross-correlation coefficient is ill defined. Rather, we will focus on testing whether there are intrinsic frequency components in SLF components that are relevant to the determination of the CI.

Acknowledgments

Appendix A

Here, we will derive a theoretical relationship between the number of time points M and the maximum-shifted cross-correlation coefficient $cc^{m}(0)$ of the two time courses $n_1(t)$ and $n_2(t)$ of white noise, with 0 as expectation and with 1 as standard deviation. The zero in $cc^{m}(0)$ represents no SLF in the time course.

Assuming that the two courses $n_1(t)$ and $n_2(t)$ have M time points and maximum time shift points T, the maximum-shifted cross-correlation is calculated as:

$$cc^{m}(0) = \max_{0 < \tau < T} \frac{1}{M} \sum_{t=1}^{M} (n_1(t) \cdot n_2(t + \tau)). \tag{A1}$$

We define $\Gamma(\tau)$ as a cross-correlation function between $n_1(t)$ and $n_2(t)$ as follows:

$$\Gamma(\tau) = \frac{1}{M} \sum_{t=1}^{M} (n_1(t) \cdot n_2(t + \tau)). \tag{A2}$$

Because it is white noise, $n(t)$ is statistically independent of $n(t+1)$. Thus, $\sum n_1(t) \cdot n_2(t)$ is independent of $\sum n_1(t) \cdot n_2(t+\tau)$ [$\tau \neq 0$, because $\sum n_1(t) \cdot n_2(t)$ is independent of $\sum n_1(t+1) \cdot n_2(t+\tau+1)$, while the latter is equal to $\sum n_1(t) \cdot n_2(t+\tau)$]. Thus, the probability function of the maximum-shifted cross-correlation coefficient is:

$$F(x|cc^{m}(0) < x) = F\left(x \Big| \max_{0 < \tau < T} \Gamma(\tau) < x\right)$$
$$= \prod_{\tau=0}^{T} F(x|\Gamma(\tau) < x)$$
$$= (F(x|\Gamma < x))^{T+1}. \tag{A3}$$

According to the Central Limit Theorem, the distribution of Γ approximates a normal distribution with a sample expectation of 0 and a sample variance of $1/M$. The probability function of Γ is:

$$F(x|\Gamma < x) = \int_{-\infty}^{x} \frac{1}{\sqrt{2\pi}\hat{\sigma}} \exp\left(-\frac{s^2}{2\hat{\sigma}^2}\right) ds \tag{A4}$$

where $\hat{\sigma} = 1/\sqrt{M}$. By substituting Eq. (A3) with Eq. (A4) and by taking the derivative, the probability density function of $cc^{m}(0)$ is:

$$p_{cc^{m}(0)}(x) = \frac{T+1}{\left(\sqrt{2\pi}\hat{\sigma}\right)^{T+1}} \left(\int_{-\infty}^{x} \exp\left(-\frac{s^2}{2\hat{\sigma}^2}\right) ds\right)^{T}$$
$$\times \exp\left(-\frac{x^2}{2\hat{\sigma}^2}\right). \tag{A5}$$

Under the present experimental conditions, T is 34 and $\hat{\sigma}$ is $1/\sqrt{180}$. The expectation of $cc^{m}(0)$ from Eq. (A5) is 0.157, and the standard deviation is 0.0362. For different time points M, there are different variances and expectations of $cc^{m}(0)$; the larger M is, the smaller are the variances and expectations. In practice, the time courses were band-pass filtered, and the data were truncated due to the shift (there will be only $M-\tau$ time points matched for cross-correlation calculation for each shift attempt), which resulted in changes shown in Fig. 2 (dark line). Table 4 further lists the detailed results to demonstrate the relationships between the number

of time points and the expectations of $cc^m(0)$ (i.e., under different conditions). An expectation of 0.23 for the simulated, truncated and filtered datasets (as shown in Table 4, row 3, column 6) is consistent with the experimental result 0.23, as shown in Table 3A, for the pure-noise region. All these results strongly support our theoretical model derived above.

In Appendix B, we will determine the minimum SNR in the voxel time courses required, which reliably obtains $cc^m(\infty)$, resulting from SLF components instead of noise. With the signal–noise model of Eq. (1), the maximum-shifted cross-correlation between two measured voxel time courses can be written as:

$$cc^m(\hat{\sigma}_s) = \frac{1}{\hat{\sigma}_s^2 + 1} \max_\tau$$
$$\times \left(\frac{1}{M} \sum_t ((s(t) + n_1(t)) \cdot (s(t+\tau) + n_2(t+\tau))) \right)$$
$$= \frac{1}{M(\hat{\sigma}_s^2 + 1)} \max_\tau$$
$$\times \left(\sum_t s(t)s(t+\tau) + \sum_t s(t)n_2(t+\tau) \right.$$
$$\left. + \sum_t s(t+\tau)n_1(t) + \sum_t n_1(t)n_2(t+\tau) \right). \quad (A6)$$

Assuming that the SLF components in both voxel time course are the same stationary $s(t)$, the sample standard deviation of $s(t)$ is $\hat{\sigma}$, the expectation is 0 and the noise $n_1(t)$ and $n_2(t)$ are both white noise with a standard deviation of 1. When the length of the time course is infinite $M \to \infty$, only the first item will remain and the other terms will approach zero. Assuming that the SLF components are stationary, the correlation function $R_{ss}(\tau)$ can be written:

$$R_{ss}(0) \geq R_{ss}(\tau) = \frac{1}{M} \sum_t s(t)s(t+\tau). \quad (A7)$$

However, when M is finite and the SNR is small, there is the possibility that experimentally obtained $R_{ss}(0)$ may not reflect the synchrony between SLF components, which means that shifting the time course may not reach the maximum synchrony among the signals. To avoid such a confounding factor, $R_{ss}(\tau)$ must be dominant in Eq. (A7), that is:

$$R_{ss}(0) \geq R_{ss}(\tau) \geq A = \left(\max_\tau \left(\frac{1}{M} \sum_t s(t)n_2(t+\tau) \right. \right.$$
$$+ \frac{1}{M} \sum_t s(t+\tau)n_1(t)$$
$$\left. \left. + \frac{1}{M} \sum_t n_1(t)n_2(t+\tau) \right) \right). \quad (A8)$$

Considering that the maximum summation of the three terms in Eq. (A7) is usually equal to or smaller than the

summation of their individual maxima, we make a more restrictive requirement by letting $R_{ss}(0)$ satisfy Eq. (A7):

$$R_{ss}(0) \geq B = \max_\tau \left(\frac{1}{M} \sum_t s(t)n_2(t+\tau) \right)$$
$$+ \max_\tau \left(\frac{1}{M} \sum_t s(t+\tau)n_1(t) \right)$$
$$+ \max_\tau \left(\frac{1}{M} \sum_t n_1(t)n_2(t+\tau) \right) \geq A. \quad (A9)$$

Assuming that the distribution of B has an upper limit of $E(B) + 3\sqrt{\text{var}(B)}$, an approximation of Eq. (A9) is:

$$R_{ss}(0) > E(B) + 3\sqrt{\text{var}(B)}. \quad (A10)$$

Based on the premise of independence between signal and noise, $s(t)n_1(t)$ will be independent of $s(t)n_2(t)$. The distribution of $\max_\tau \left(\frac{1}{M} \sum_t s(t)n_2(t+\tau) \right)$ is similar to that of $\max_\tau \left(\frac{1}{M} \sum_t n_1(t)n_2(t+\tau) \right)$. Two terms on the right side of Eq. (A10) can be respectively expressed as:

$$E(B) = 2E \left(\max_\tau \left(\frac{1}{M} \sum_t s(t)n_2(t+\tau) \right) \right)$$
$$+ E \left(\max_\tau \left(\frac{1}{M} \sum_t n_1(t)n_2(t+\tau) \right) \right)$$
$$\text{Var}(B) = 2\text{Var} \left(\max_\tau \left(\frac{1}{M} \sum_t s(t)n_2(t+\tau) \right) \right)$$
$$+ \text{Var} \left(\max_\tau \left(\frac{1}{M} \sum_t n_1(t)n_2(t+\tau) \right) \right). \quad (A11)$$

By using the experimental parameters T (=34) and M (=180) in Eq. (A5), we obtain sample estimations of $E(Q)$ and $\text{var}(Q)$:

$$\hat{E}(B) = 0.314\hat{\sigma}_s + 0.157, \text{var}(\hat{B}) = 0.00262\hat{\sigma}_s^2 + 0.00131. \quad (A12)$$

Substituting Eq. (A10) with Eq. (A12), we obtain:

$$\hat{\sigma}_s^2 > 0.314\hat{\sigma}_s + 0.157 + 0.1086\sqrt{2\hat{\sigma}_s^2 + 1}. \quad (A13)$$

By solving the above inequality with a simulation, the threshold of the SNR is determined to be 0.74. Considering the effects of the truncation and the Hamming filter, Eq. (A13) becomes:

$$\hat{\sigma}_s^2 > 0.46\sigma_s + 0.23 + 0.2064\sqrt{2\hat{\sigma}_s^2 + 1}. \quad (A14)$$

The solution of Eq. (A14) is:

$$\eta = \hat{\sigma}_s > 1.036. \quad (A15)$$

Again, the noise variance is 1. Eq. (A15) suggests that with the SNR being larger than 1.036, the maximum-shifted cross-correlation coefficient resulted from the
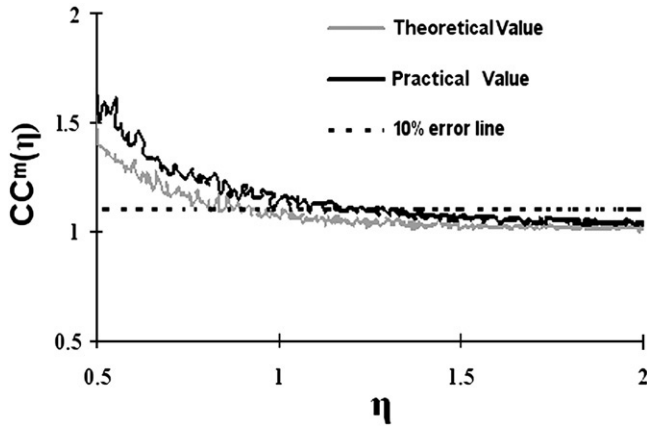
Fig. 3. The normalized maximum-shifted cross-correlation coefficient $cc^m(\eta)$ versus η. The lighter gray line represents theoretical values based on Eq. (A15), and the dark line represents practical values after truncation and filtering. The dashed line represents a threshold of 10% error in $cc^m(\eta)$ at $\eta=1.036$. The smaller η is, the bigger is the error in $cc^m(\eta)$, and vice versa.

synchrony of SLF components rather than from noise. Based on the analytical solution in Eq. (A14), the minimum required SNR of 1.036 would produce about 10% error, as simulated in Fig. 3. The simulation was made with the assumption that both SLF components are of the same sine waves, with a frequency of 0.0575 Hz (center of the low-frequency band, 0.015–0.1 Hz) and with different levels of SNR. Clearly, if the SLF contains multiple frequency components, the required SNR for the same error level will be higher.

Appendix B

To validate the approximation in Eqs. (6) and (8), where the SNR $\hat{\eta}$ is assumed to be identical in all voxel time courses within an ROI, and to compare the nCI calculated from Eqs. (6) and (8) to the oCI calculated from Eq. (3), the simulations are constructed as follows. The voxel time course from the ith voxel is expressed as in Eq. (9). For benchmark comparison, we have also constructed a hypothetical noise-free ROI with the voxel time course as:

$$u_i(t) = \sqrt{2}\sin(2\pi f_c t + \theta_i). \tag{B1}$$

Three sets of simulations are implemented to examine the impact of SNRs on (a) the oCI based on Eq. (3); (b) the nCI based on Eq. (6); and (c) approximately normalized CI (anCI) based on Eq. (8). Three sets of normal SNR distributions are defined as $N_1(1.75, 0.25^2)$, $N_2(2.5, 0.5^2)$ and $N_3(4, 1^2)$ based on a reasonable representation of substantial SNR variations that are observed across the hippocampus. In addition, the means and standard deviations of the SNR distributions are set to satisfy a minimum SNR of mean±3S.D.≥1, as described in Appendix A. θ_i is the phase that also obeys a
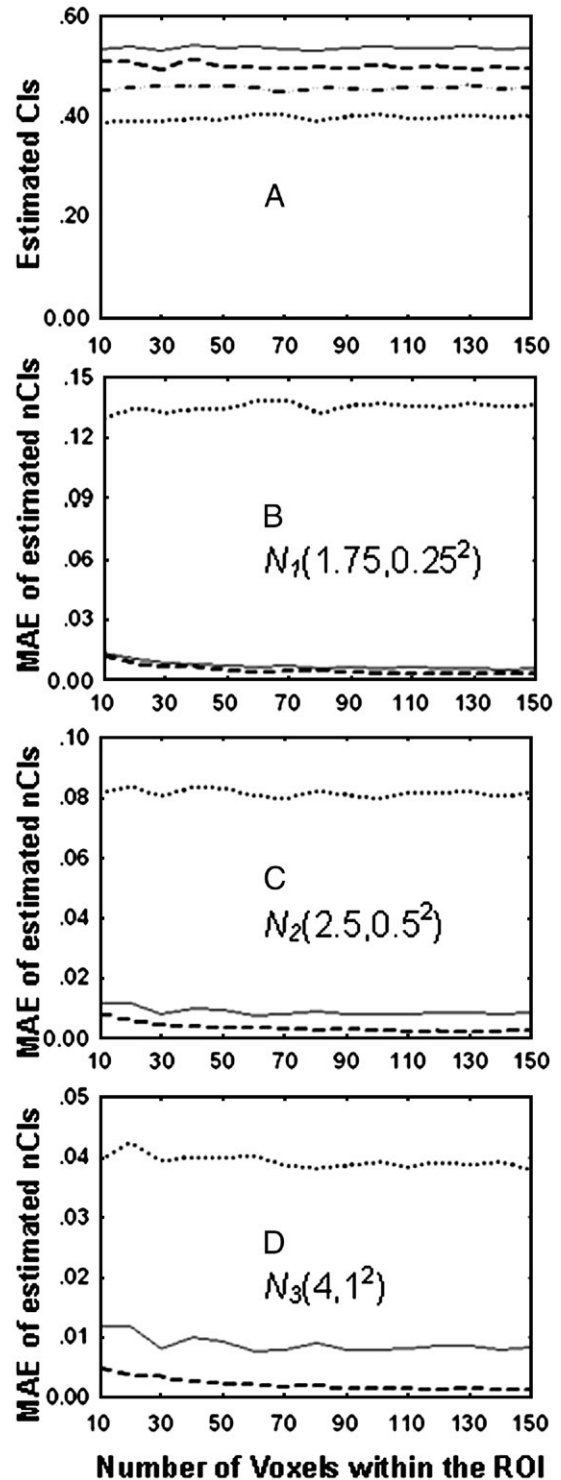

Fig. 4. Simulation of the independence of the nCI from different SNRs. (A) Four sets of simulations are implemented to examine the impact of different SNRs on the oCI based on Eq. (3). The solid line, dashed line, dash-dotted line and dotted line represent the oCI in different noise distributions at noise-free $N_1(1.75, 0.25^2)$, $N_2(2.5, 0.5^2)$ and $N_3(4, 1^2)$, respectively. (B–D) The MAEs of oCI (dotted line) and nCI (dashed line) based on Eq. (6), and the MAE of anCI (solid line) based on Eq. (8) at three different SNR distributions.
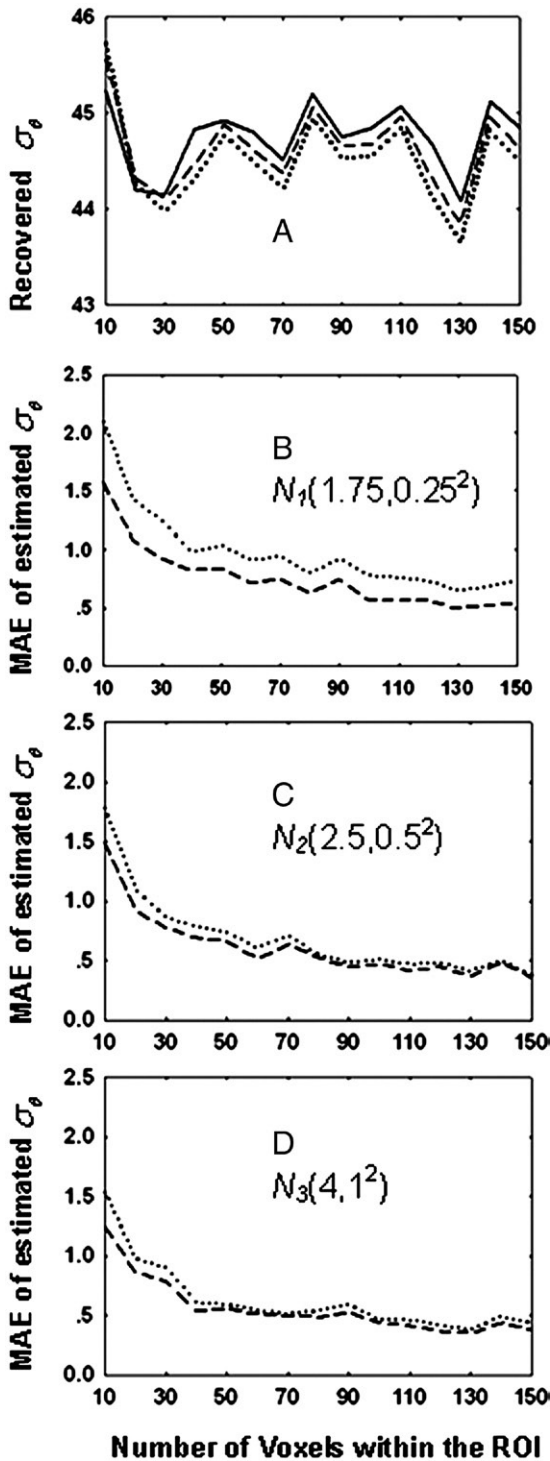
Fig. 5. Simulation of the independence of the PSI estimation from the SNRs. (A) Three sets of simulations are implemented to examine the impact of the approximation between Eqs. (14) and (15) in the case of the noise-free condition. The solid line, dashed line and dotted line represent the given σ_θ and the estimated $\hat{\sigma}_\theta$ from Eqs. (14) and (15), respectively. (B–D) The MAEs of estimated $\hat{\sigma}_\theta$ based on Eq. (14) (dotted line) and Eq. (15) (dashed line) at three different SNR distributions. The vertical units for (A)–(D) are all expressed in degrees.

Table 5
Statistical significance of σ_θ calculated from Eq. (B8) based on θ_G calculated from Eq. (15) in the hippocampal region of three subject groups

(A) Recovered σ_θ (mean±S.D.)

Region	AD	MCI	Control
Hippocampus^{nr}	59.07±10.48	46.03±5.36	30.30±6.81
Hippocampus^{rg}	54.99±12.99	49.00±7.33	32.78±8.61

(B) One-way unbalanced ANOVA for the σ_θ of three subject groups

Parameter	$F_{nr}(2,23)$	P_{nr}	$F_{rg}(2,23)$	P_{rg}
σ_θ	26.209	<.0001	10.392	.0006

(C) Pairwise (one-tailed) t test between three subject groups

Group	P
σ_θ^{nr}	
AD vs. MCI **	.0042
MCI vs. CONTROL **	.0008
AD vs. CONTROL ***	<.0001
σ_θ^{rg}	
AD vs. MCI	.2594
MCI vs. CONTROL **	.0047
AD vs. CONTROLL ***	.0002

(D) Kruskal–Wallis nonparametric tests for the σ_θ of three subject groups

Parameter	H_{nr}	P_{nr}	H_{rg}	P_{rg}
σ_θ	17.939	.0001	11.478	.0032

nr — no CSF voxel regression; rg — with CSF voxel regression.
  *P<05.
  ** P<01.
  *** P<001.

normal distribution and is set to be $N(0,(\pi/4)^2)$, according to a previous study [21]; f_c is a predefined frequency (0.0575 Hz), which is the middle frequency of SLF components between 0.015 and 0.1 Hz; $n_i(t)$ is the normally distributed thermal noise; and η_i, θ_i and $n_i(t)$ are independent of one another. The time length is 6 min, and the sampling frequency is 0.5 Hz, which corresponds to a T_R of 2 s.

In each set of SNR distribution, we perform Monte Carlo simulations by altering the SNRs and the number of voxels in an ROI from 10 to 150, with 10 as increment. At a given voxel number, each voxelwise SNR level was randomly generated within a given SNR distribution. This procedure was independently repeated for 100 times. Then, the 100 estimations obtained of the CI were averaged to yield a final simulated estimation. To evaluate the simulation performance, we employed the mean absolute error (MAE), as calculated below:

$$\text{MAE} = \frac{1}{L}\sum_{l=1}^{L} |V_l - V_0| \qquad (B2)$$

where V_l represents the CI in each case of calculation (oCI, nCI or anCI) obtained from Eq. (3), Eq. (6) or Eq. (8), respectively, at a given voxel number and SNR distribution; L is equal to 100 as a trial repetition; and V_0 represents the CI calculated from Eq. (B1) without noise.

Fig. 4 shows the simulated results between the different levels of SNR distribution and the estimated CI at different numbers of voxels. Fig. 4A demonstrates that, without noise, the oCI is 0.538±0.003. With the SNR distributions of $N_1(1.75,0.25^2)$, $N_2(2.5,0.5^2)$ and $N_3(4,1^2)$, the oCIs are 0.399±0.004, 0.456±0.008 and 0.501±0.007, respectively. Clearly, the SNR significantly affects the CI estimation. When the SNR distribution is normalized, the accuracy of the CI estimation is significantly improved, as shown in Fig. 4B–D. Specifically, Fig. 4B shows that with an SNR distribution of $N_1(1.75,0.25^2)$, the MAE is 0.135±0.002 for oCI, 0.005±0.002 for nCI and 0.007±0.002 for anCI. Clearly, the MAE is largest for the oCI calculation, based on Eq. (3), in contrast to the nCI estimated by Eqs. (6) and (8). Furthermore, Fig. 4B shows that the assumption made from Eq. (6) to Eq. (8) is statistically valid, since the difference is only 0.002. The MAE of 0.002, compared to the no-noise case of the CI (0.538±0.003), only represents 0.4%. Similarly, with an SNR distribution of $N_2(2.5,0.5^2)$, as shown in Fig. 4C, the corresponding MAEs are 0.082±0.002 for oCI, 0.003±0.001 for nCI and 0.009±0.001 for anCI. With an SNR distribution of $N_3(4,1^2)$, as shown in Fig. 4D, the corresponding MAEs are 0.038±0.001 for oCI, 0.002±0.001 for nCI and 0.007±0.001 for anCI. These data not only demonstrate how the different SNRs affect the oCI estimation but also prove that normalization of the CI is an optimal estimation. In addition, these data also validate our approximation from Eq. (6) to Eq. (8), with a mean SNR over an ROI. This assumption not only significantly reduced the computational cost but also provided an accurate estimation of the nCI.

To validate PSI's independence of SNRs and the approximation in Eqs. (14) and (15), the same datasets of the simulations and procedures described above were employed. These were contained in three different SNR distributions $N_1(1.75,0.25^2)$, $N_2(2.5,0.5^2)$ and $N_3(4,1^2)$, and a phase distribution $N(0,\sigma_\theta^2)$, where σ_θ is set to $(\pi/4)$. Similarly, the MAE was employed to quantify the error between the given phase distribution and the calculated PSI with Eqs. (14) and (15). As shown in Fig. 5A, when using the noise-free SLF signal based on Eq. (B1), both PSI measurements with Eqs. (14) and (15) provided accurate detection of the input phase σ_θ, which is set to $\pi/4$ (45°). When the SNR distribution is set to $N_1(1.75,0.25^2)$ and the ROI is 10, the MAE of PSI from Eq. (14) is 2.09° and that from Eq. (15) is 1.6° (Fig. 5B). The PSI estimation based on Eq. (15) is more accurate than the approach based on Eq. (14). As shown in Fig. 5B–D, the larger an ROI is, the more accurate is the PSI estimation. For example, when voxels in an ROI are >100, the MAE is about 0.5° for both estimations. These simulations validate our assumption between Eqs. (14) and (15).

It should be pointed out that the calculated $\hat{\theta}_G$ from Eq. (14) is not directly equal to σ_θ and that they have a relationship:

$$\hat{\theta}_G = \frac{2}{\sqrt{\pi}\sigma_\theta}. \tag{B3}$$

To derive this relationship, we restate the phase distribution in the voxel time courses as $N(\theta_0,\sigma_\theta^2)$ and assume that the phase of each voxel within the ROI is $(\theta_1,\theta_2,\ldots,\theta_K)$. Based on Eq. (14):

$$\hat{\theta}_{G(Eq.\ (14))} = \frac{2}{K(K-1)} \sum_{i,j=1,i\neq j}^{K} \left| \theta_{ij}^d \right|$$
$$= \frac{2}{K(K-1)} \sum_{i,j=1,i\neq j}^{K} \left| \theta_i - \theta_j \right| \tag{B4}$$

where $\theta_{ij}^d = \theta_i - \theta_j \sim N(0,2\sigma_\theta^2)$, and the SNR item is cancelled due to the ratio between the cross-correlation coefficient and the maximum-shifted cross-correlation coefficient. Therefore, the PSI within the region turns out to be:

$$\hat{\theta}_{G(Eq.\ (14))} = \langle |\theta_{ij}^d| \rangle \approx \int_{-\infty}^{\infty} |t| \cdot \frac{1}{2\sigma_\theta\sqrt{2\pi}} \cdot e^{-\frac{t^2}{4\sigma_\theta^2}} dt$$
$$= \frac{1}{\sqrt{2\pi}\sigma_\theta} \int_0^{\infty} t \cdot e^{-\frac{t^2}{4\sigma_\theta^2}} dt = \frac{2}{\sqrt{\pi}}\sigma_\theta \tag{B5}$$

as shown in Eq. (B3) above. Similarly, the $\hat{\theta}_G$ calculated from Eq. (15) and σ_θ have the following relationship and can be derived as:

$$\cos(\theta_{G(Eq.\ (15))}) = \frac{CI}{CI^m}$$
$$= \frac{\frac{2}{K(K-1)} \sum_{1\leq i<j\leq K} \left(\frac{\eta_i}{\sqrt{\eta_i^2+1}} \cdot \frac{\eta_j}{\sqrt{\eta_j^2+1}} \cdot \cos(\theta_i - \theta_j) \right)}{\frac{2}{K(K-1)} \sum_{1\leq i<j\leq K} \left(\frac{\eta_i}{\sqrt{\eta_i^2+1}} \cdot \frac{\eta_i}{\sqrt{\eta_j^2+1}} \right)}$$
$$= \frac{\frac{2}{K(K-1)} \sum_{1\leq i<j\leq K} \left(\tilde{\eta}_i \cdot \tilde{\eta}_j \cdot \cos(\theta_i - \theta_j) \right)}{\frac{2}{K(K-1)} \sum_{1\leq i<j\leq K} \left(\tilde{\eta}_j \tilde{\eta}_j \right)} \approx \frac{\overline{\tilde{\eta}_i \cdot \tilde{\eta}_j \cdot \cos(\theta_i - \theta_j)}}{\overline{\tilde{\eta}_i \cdot \tilde{\eta}_j}} \tag{B6}$$

where $\tilde{\eta}_i = \frac{\eta_i}{\sqrt{\eta_i^2+1}}$.

The last step of the approximation in Eq. (B6) stands when the number of voxels within the ROI K is very large. As the initial assumption η_i is independent of θ_i and so is $\tilde{\eta}_i$, its mean is not zero, as predefined. Therefore, Eq. (B6) can be simplified as:

Therefore, Eq. (B6) can be simplified as:

$$\cos(\theta_{G(Eq.\ 15)}) \approx (\cos(\theta_i - \theta_j), \; 1 \leq i < j \leq K \tag{B7}$$

Use Taylor Series to expand the cosine item:

$$\cos(\theta_{G(Eq.\ (15))}) \approx \sum_{n=1}^{\infty} \frac{(-1)^n}{(2n)!} (\theta_i - \theta_j)^{2n}$$
$$\approx 1 - \frac{1}{2}(\theta_i - \theta_j)^2 + \frac{1}{24}(\theta_i - \theta_j)^4 - \frac{1}{720}(\theta_i - \theta_j)^6 + \frac{1}{40,320}(\theta_i - \theta_j)^8$$
$$= 1 - \sigma_\theta^2 + \frac{1}{2}\sigma_\theta^4 - \frac{1}{6}\sigma_\theta^6 + \frac{1}{384}\sigma_\theta^8. \tag{B8}$$

The above derivation utilizes the fact that θ_i is independent of θ_j when $i\neq j$. The high even-order moments

of θ_i, such as $E(\theta_i^4)=3\sigma_\theta^4$, $E(\theta_i^6)=15\sigma_\theta^6$ and $E(\theta_i^8)=105\sigma_\theta^8$, are obtained from the generating function of the preassumed Gaussian distribution $N(\theta_0,\sigma_\theta^2)$, and the high odd-order moments are zero. To further improve the precision of recovering σ_θ, a higher-order item in the Taylor series can be added. In practice, Eq. (B8) is sufficient and can be solved with the Aitken method.

By applying Eq. (B8) to datasets obtained from the human hippocampus in Table 3, σ_θ can be obtained from $\hat{\theta}_G$. The results are listed in Table 5, and the statistical significance values are the same as in Table 3.

References

[1] Petersen RC, Smith GE, Waring SC, Ivnik RJ, Tangalos EG, Kokmen E. Mild cognitive impairment: clinical characterization and outcome. Arch Neurol 1999;56:303–8.

[2] Petrella JR, Coleman RE, Doraiswamy PM. Neuroimaging and early diagnosis of Alzheimer disease: a look to the future. Radiology 2003; 2262:315–36.

[3] Li SJ, Li Z, Wu G, Zhang MJ, Franczak M, Antuono PG. Alzheimer's disease: evaluation of a functional MR imaging index as a marker. Radiology 2002;2251:253–9.

[4] Braak H, Braak E. Neuropathological staging of Alzheimer-related changes. Acta Neuropathol 1991;82:239–59.

[5] Buckner RL, Snyder AZ, Shannon BJ, LaRossa G, Sachs R, Fotenos AF, et al. Molecular, structural, and functional characterization of Alzheimer's disease: evidence for a relationship between default activity, amyloid, and memory. J Neurosci 2005;25:7709–17.

[6] Krüger G, Glover GH. Physiological noise in oxygenation-sensitive magnetic resonance imaging. Magn Reson Med 2001;46:631–7.

[7] Krüger G, Kastrup A, Glover GH. Neuroimaging at 1.5 T and 3.0 T: comparison of oxygenation-sensitive magnetic resonance imaging. Magn Reson Med 2001;45:595–604.

[8] Peltier SJ, Noll DC. T_2^* dependence of low-frequency functional connectivity. Neuroimage 2002;16:985–92.

[9] Cox RW. AFNI: software for analysis and visualization of functional magnetic resonance neuroimages. Comput Biomed Res 1996;29: 162–73.

[10] Duvernoy HM. The human hippocampus: functional anatomy, vascularization and serial sections with MRI. 2nd ed. New York: Springer; 1998.

[11] Lowe MJ, Russell DP. Treatment of baseline drifts in fMRI time series analysis. J Comput Assist Tomogr 1999;23(3):463–73.

[12] Gudbjartsson H, Patz S. The Rician distribution of noisy MRI data. Magn Reson Med 1995;34:910–4.

[13] Cordes D, Haughton VM, Arfanakis K, Wendt GJ, Turski PA, Moritz CH, et al. Mapping functionally related regions of brain with functional connectivity MR imaging. AJNR Am J Neuroradiol 2000; 21:1636–44.

[14] Thirion B, Dodel S, Poline JB. Detection of signal synchronizations in resting-state fMRI datasets. Neuroimage 2006;29:321–7.

[15] Sun FT, Miller LM, D'Esposito M. Measuring temporal dynamics of functional networks using phase spectrum of fMRI data. NeuroImage 2005;28:227–37.

[16] Glover GH, Li TQ, Ress D. Image-based method for retrospective correction of physiological motion effects in fMRI: RETROICOR. Mag Reson Med 2000;44:162–7.

[17] Hu X, Le TH, Parrish T, Erhard P. Retrospective estimation and correction of physiological fluctuation in functional MRI. Mag Reson Med 1995;34:201–12.

[18] Zhao X, Bodurka J, Jesmanowicz A, Li SJ. B_0-fluctuation-induced temporal variation in EPI image series due to the disturbance of steady-state free precession. Magn Reson Med 2000;44:758–65.

[19] Birn RM, Diamond JB, Smith M, Bandettini PA. Separating respiratory-variation-related fluctuations from neuronal-activity-related fluctuations in fMRI. Neuroimage 2006;31:1536–48.

[20] Wise RG, Ide K, Poulin MJ, Tracey I. Resting fluctuations in arterial carbon dioxide induce significant low-frequency variations in BOLD signal. NeuroImage 2004;21:1652–64.

[21] Xu G, Xu Y, Wu G, Antuono PG, Hammeke TA, Li SJ. Task-modulation of functional synchrony between spontaneous low-frequency oscillations in the human brain detected by fMRI. Magn Reson Med 2006;56:41–50.